The effect of variable nozzle temperature and cross-sectional pattern on interlayer tensile strength of 3D printed ABS specimens

M. Foppiano, A. Saluja, K. Fayazbakhsh*

Department of Aerospace Engineering, Ryerson University, Toronto, Ontario M5B2K3, Canada

*Corresponding author: kazem@ryerson.ca; Tel: (+1) 416-979-5000 ext. 556414; fax: (+1) 416-979-5056; https://orcid.org/0000-0003-3963-8282

Abstract

Background: Fused filament fabrication (FFF) introduces anisotropic material properties to the final parts, which includes minimum interlayer values. In this study, ASTM D638 type I specimens are 3D printed from acrylonitrile butadiene styrene (ABS) in the upright build direction and their tensile properties are evaluated. ***Objective***: Higher nozzle temperature outside the narrow section is proposed to improve tensile properties and move the breakage location towards the specimen center. Time spent above the glass transition temperature in the specimens is suggested as an indicator of their local strength. ***Methods***: An enclosure is built for a LulzBot Taz 6 desktop 3D printer that allows thermal imaging without interference from the environment. Temperature and humidity inside and outside the enclosure, and specimen mass are recorded. An automation script is developed to extract the temperature history of the deposited layers during 3D printing along the specimens. ***Results***: Optimum cross-sectional pattern for maximum tensile properties is the one with all walls and no infill. Nozzle temperature is varied from 220 to 260 °C in 10°C increments and 231 °C is found as optimum for highest tensile properties. Using the optimum nozzle temperature of 231 °C in the narrow section, and a higher temperature of 261 °C in the grip sections and transition areas moves the breakage location towards the specimen center. ***Conclusions***: Time spent above the glass transition temperature agrees well with breakage location of the specimens. The impact of humidity on tensile properties is found to be more pronounced than the specimen mass.

Keywords: Interlayer tensile strength; Thermal imaging; Fused filament fabrication; Temperature history; Tensile properties

Experimental Mechanics

https://doi.org/10.1007/s11340-021-00757-y

1. Introduction

Fused filament fabrication (FFF) is a popular 3D printing technique that can process a wide range of feedstock materials, mainly pure polymers, and in general is less expensive and more suitable for large-scale manufacturing compared to other 3D printing methods. An abundance of research studies explored different design and manufacturing parameters to increase structural performance of FFF 3D printed parts. Tensile properties have been the focus for many researchers, and they followed ASTM D638 or ISO 527-2 standards. They investigated the impact of a wide range of parameters, including build orientation, nozzle temperature, bed temperature, layer thickness, raster angle, printing speed, cooling, and infill [1, 2]. It was found that the build orientation has a significant impact on final tensile properties, where 3D printed specimens in the upright direction (ZXY/ZYX) exhibited the lowest values compared to the ones manufactured on-edge (XZY/YZX) and flat (XYZ/YXZ). As a result, improving interlayer tensile strength of FFF 3D printed parts from pure polymers is critical for their widespread application.

Rane et al. [3] explored thermal annealing to improve tensile strength of FFF 3D printed specimens per a modified version of ASTM D638 standard. To prevent distortion of specimens during the annealing process, they custom-built a fixture with aluminum separators and side supports for the specimens. They explored four annealing temperature of 120, 140, 160, and 180 °C, and compared the tensile strength of their respective treated specimens with the baseline, no annealing. They found an increase of 89 % in tensile strength of specimens annealed at 160 °C compared to the baseline. Additional fixture and the annealing process increase the final part cost and production time, which eliminates the savings from the 3D printing technique. Lin et al. [4] 3D printed multi-materials specimens (PCL above PLA) per a modified version of ASTM D638 standard in the upright direction. They proposed a single-layer temperature-adjusting transition (SLTAT) method,

in which they changed the bonding-layer temperature from 90 to 210 °C in 20 °C increments, while the rest of layers were extruded at their usual temperature of 210 and 110 °C for PLA and PCL, respectively. They reported a 28 % improvement in tensile strength for specimens with bonding-layer temperature of 130 °C compared to the baseline.

Zaldivar et al. [5] exposed the ULTEM® 9085 filament to humidity conditions to achieve 0, 0.05, 0.1, 0.16, 0.4, and 0.8 % humidity by wight. They used a Stratasys Fortus 900MC and 3D printed ASTM D638 type I specimens in the flat (XYZ) and the upright (ZXY) directions. With an increase in the humidity levels, they found a decrease in all tensile properties of the ZXY specimens. For the highest humidity level investigated for the ZXY specimens, 0.16 wt.%, they observed a 42.1 %, 11.5 %, and 44.4 % reduction in tensile strength, modulus, and failure strain, respectively, compared to the baseline. They attributed this decrease to higher trapped porosity and flow characteristics of the extruder not being optimum for a filament with a high humidity level. Even though they did not report specimen weights, a not-optimized extrusion parameters might result in lower specimen weights compared to the ideal case, which in turn results in lower tensile strength as reported by Tanikella et al. [6].

Several researchers investigated the impact of interlayer cooling on mechanical properties of FFF 3D printed parts. Faes et al. [7] 3D printed ISO 527 specimens in the flat (YXZ) and the upright directions (ZXY) using a Stratasys Dimension SST 1200es from acrylonitrile butadiene styrene (ABS). They introduced interlayer cooling by changing the number of specimens being 3D printed simultaneously. For the ZXY specimens, they 3D printed 1, 2, 3, 5, and 10 specimens simultaneously and found the maximum drop in tensile properties for 10 specimens in the envelope. Tensile strength, modulus, and failure strain were decreased by 35.1 %, 4.5 % and 28.9 %, respective, compared to one specimen in the envelope, the baseline. 3D printing multiple

specimens at the same time might introduce defects into the parts because of the nozzle movement between them. Morales et al. [8] 3D printed true compression (TC) and shear compression (SC) specimens at five different interlayer wait times of 0, 5, 10, 15, and 20 s. For both TC and SC specimens, there was little variation in compressive modulus between different wait times, while compressive strength reduced significantly by increasing the wait time. They observed a maximum of 12 % and 25 % reduction in compressive strength for TC and SC specimens, respectively.

Previous research works [3-7] used dog-bone tensile specimens 3D printed in the vertical direction for the evaluation of interlayer tensile strength. Other researchers reported often high variability in tensile results for these types of specimens and frequent failures in their transition area [9, 10]. To mitigate these risks, Kuznetsov et al. [11] first proposed a tube with a rectangular cross section loaded in 3-point bending test as an indication for interlayer tensile strength. The investigated the impact of the filament pigmentation, nozzle diameter, and layer thickness on the ultimate fracture strength (UFS). They found that natural filament (no pigmentation) had slightly better strength, and there is a positive relation between specimen strength and nozzle diameter, while this is the reverse for layer thickness. In a follow-up study [12], they studied temperature-related process parameters, i.e., extrusion temperature, cooling intensity, printing speed, and layer printing time. By an increase in the extrusion temperature, there was an increase in UFS, specimen mass, and sublayer temperature (t_{SUB}). As expected, fan speed (0 to 100 %) and layer printing time had an inverse relation with UFS and t_{SUB}. An increase in feed rate generally resulted in an increase in UFS and t_{SUB}, while it reduced specimen mass. They generalized and described the impact of these four process parameters on the UFS by extrusion efficiency (E_E) and t_{SUB}. An increase in both E_E and t_{SUB} results in an increase in the UFS, which signifies the optimization of FFF 3D printing process parameters for improved interlayer tensile strength. Finally, the authors studied four

commercial desktop FFF 3D printers, and explored the impact of layer thickness and printing speed on the UFS, specimen mass, and t_{SUB} [13]. The maximum UFS recorded for all machines were similar (47 ± 2.5 MPa); however, for the same layer thickness and printing speed, the UFS and specimen mass were varied among different machines. They found that t_{SUB} also varied significantly due to differences in enclosures and cooling system designs. They found no significant difference in results due to filament diameter (1.75 versus 2.85 mm) or motion systems (Cartesian versus Delta). They also used an Ultimaker 2 frame and installed a suspended 1.75 mm extruder, and reached a maximum UFS of 65.8 MPa, which is 40 % improvement over the commercial desktop 3D printers. They concluded that the machine hardware can drastically change the impact of the process parameters and previous findings cannot be generalized to any machine setup.

The tubular specimen used by Kuznetsov et al. [11-13] is not per a standardized testing technique and the resulting ultimate fracture strength cannot be used as a strength property in simulation models. In addition, they did not record humidity conditions during 3D printing that can significantly impact the interlayer tensile strength [5]. While they used infrared (IR) thermography, which was not completed in the other studies described here [3-8], only an average temperature over an area between 1 and 3 mm from the nozzle at a specific time was reported. Furthermore, they used a constant nozzle temperature throughout a whole specimen fabrication and did not adjust it. The commercial desktop 3D printers investigated in the previous discussed studies were not fully enclosed [4, 6, 9], which accelerated the cooling of deposited layers and induced internal defects into the specimens.

Ferrell et al. [14] found that failure location, e.g., at the transition area of an ASTM D638 type V specimen, had no effect on the specimen ultimate tensile strength and Young's modulus. As a

result, the downside of using a dog-bone tensile specimen is limited considering its advantage of evaluating material properties that can be fed into simulation models. Here, a LulzBot Taz 6 FFF 3D printer with a custom-built enclosure is used to manufacture ASTM D638 type I specimens from ABS in the upright build direction to investigate their interlayer tensile strength. Humidity and temperature inside and outside the enclosure are monitored, and thermal images are taken during specimen 3D printing. First, cross-sectional pattern is optimized for the specimens, which has not been investigated in the past, and is followed by an investigation of the optimum nozzle temperature. Then, variable nozzle temperature through the specimen length is proposed as a novel solution to move the breakage location towards the narrow section. At the end, the complete temperature history of deposited layers during 3D printing is found for the first time and its relationship to breakage location is investigated. The paper wraps up with the main conclusions and directions for future work.

2. Methodology

2.1. Specimen design

Manufacturing and design parameters affect interlayer tensile strength, dimensional accuracy, and printing time of 3D printed parts. Specimens per ASTM D638-14 standard type I are 3D printed in ZXY build orientation (upright) and are tested to obtain their tensile properties. It is proposed that the interlayer tensile strength could be improved by increasing the nozzle temperature for regions that have larger surface areas. This way, the nozzle temperature in the grip regions and transition areas (T_1) is higher than the narrow section (T_0) of the specimen. Figure 1 shows dimensions of the specimen per the standard and the nozzle temperature variation along the

specimen length. It should be noted that breakage inside the narrow section of the specimen is considered acceptable per ASTM D638-14.

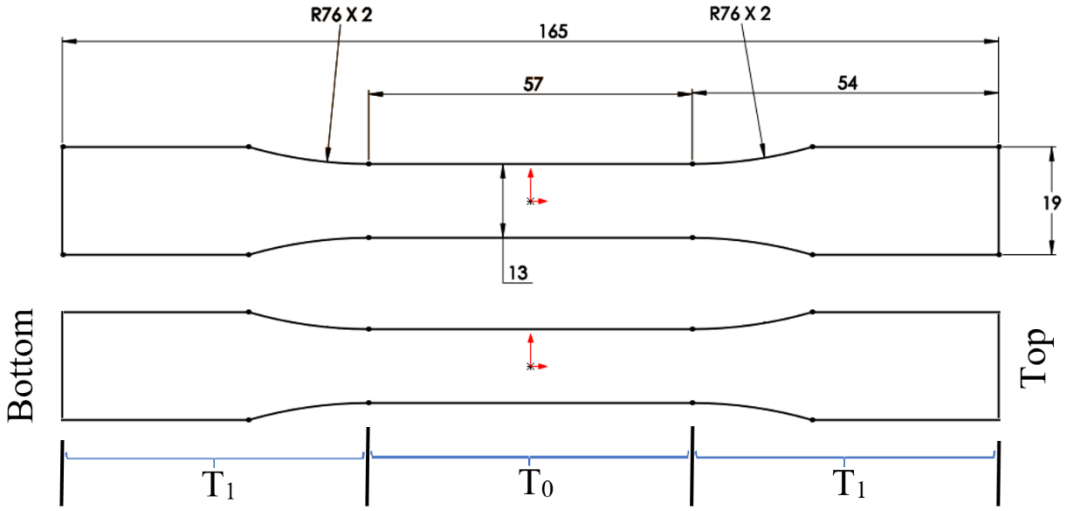

Figure 1. Specimen dimensions in mm and the nozzle temperature variation along the length.

A naming convention is used in this investigation to distinguish specimens and has the following format: Tz-XX-X. The "Tz" refers to the LulzBot Taz 6 printer, and the first two digits (XX) refer to a unique Gcode for a specific set of 3D printing process and design parameters for each experiment, while the last digit corresponds to the specimen number in the same experiment.

Table 1 summarizes process parameters for three sets of trials planned and conducted in this study. The first set (Tz-1-1, 2-1, 3, 4, 5-1, and 6-1) explores different printing patterns, which results in four different cross sections, and their impact on tensile properties of the specimens. Printing patterns significantly affect interlayer tensile strength and have not been investigated in the literature. It should be noted that the printing pattern is independent of the nozzle temperature and a change in temperature would not influence its results. Figure 2 is the visualization of the cross sections for layer one of the specimens obtained from Simplify3D version 4.1.2. Different wall thickness values and printing patterns resulted in four different cross-sectional patterns, a to d. It should be noted that cross-sectional patterns a (in to out) and b (out to in) after 3D printing look

the same, which can be seen as three rectangles, inside, middle, and outside (Figure 2). However, they are 3D printed in different manners. In printing pattern a, first, the inside rectangle is completed followed by the middle and the outside rectangles. While for printing pattern b, manufacturing starts from the outside rectangle and 3D printing continues with the middle and inside rectangles. Once the optimum printing pattern is determined, it is used to find optimum nozzle temperature in the narrow section (T_0) of the specimen. If the temperature is set too low, it will result in a weak bond between deposited layers and the surface could be a bit rough. On the other hand, too high a temperature may cause polymer degradation and more defects in the 3D printed parts. It will reduce the polymer viscosity drastically causing the molten material to leak out from the nozzle during manufacturing [1]. Here, the nozzle temperature is varied from 220 to 260 °C in 10-degree increments to find ideal nozzle temperature for maximum tensile properties (Tz-7 to 10). In the last set of experiments (Tz-11 to 15), the optimum printing pattern from the first set of trials is considered and the optimum nozzle temperature from the second experimental case is used in the narrow section of the specimens. However, a higher nozzle temperature is used in the grip sections and transition areas, as indicated in Figure 1. It should be noted that the Tz-8 specimens from the second set have a constant nozzle temperature of 230 °C along their length (no temperature gradient) and can be considered as a baseline for comparison with specimens from the last set that have temperature gradient of 5, 10, 15, 20, and 30 °C.

Table 1. Process parameters for 3D printing trials.

Run/Gcode name	Wall thickness (mm)	Printing pattern	Cross-sectional pattern	Nozzle temperature (°C)	Temperature gradient (°C)	Slicer print time (min)
Tz-1-1[1]	1.5	in to out	a	240		110
Tz-2-1	1.5	in to out	a	240		110
Tz-3 [2]	1.5	in to out	a	240		128
Tz-4 [3]	1.5	out to in	b	240		128
Tz-5-1[4]	0	infill	d	240		127

Tz-6-1	0.5	infill	c	240		148
Tz-7 [5]	1.5	in to out	a	220		128
Tz-8 [6]	1.5	in to out	a	230		128
Tz-9 [3]	1.5	in to out	a	250		128
Tz-10 [3]	1.5	in to out	a	260		128
Tz-11 [3]	1.5	in to out	a	231	5	128
Tz-12 [6]	1.5	in to out	a	231	10	128
Tz-13 [3]	1.5	in to out	a	231	15	128
Tz-14 [3]	1.5	in to out	a	231	20	128
Tz-15 [3]	1.5	in to out	a	231	30	128

[1] Fan cooling was enabled; [2] Total of 8 specimens printed and tested successfully; [3] Total of 5 specimens printed and tested successfully; [4] Extra skin wall count of 1 as opposed to 0 for all the other specimens; [5] Total of 3 specimens printed and tested successfully; [6] Total of 4 specimens printed and tested successfully.

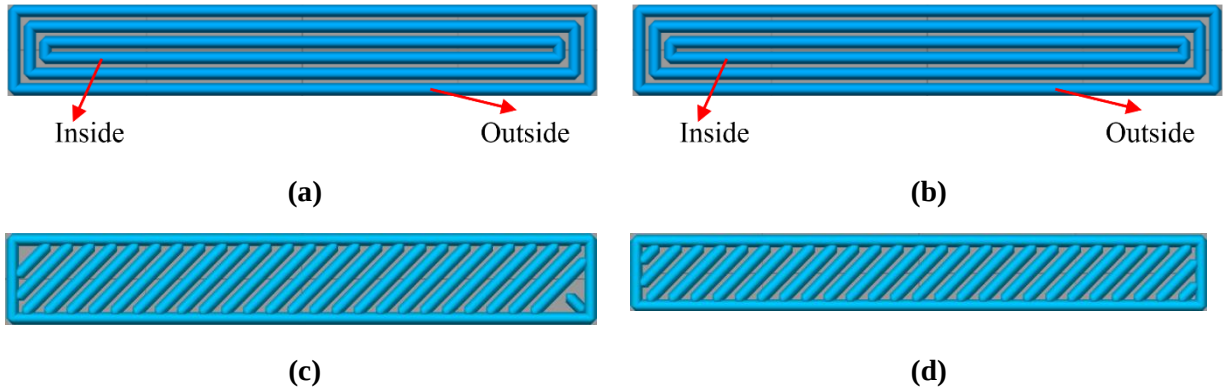

Figure 2. Cross-sectional pattern of 3D printed specimens with different wall thickness and printing pattern: (a) 1.5 mm, in to out; (b) 1.5 mm, out to in; (c) 0.5 mm, extra skin off; and (d) 0 mm, extra skin on.

2.2 Specimen manufacturing

Specimens were 3D printed in the ZXY build direction (upright) per ASTM D638 type I with a nominal total thickness of 3.30 mm. Transparent ABS feedstock procured from Filaments.ca from one batch (batch# BH10CE) was used for manufacturing. A Lulzbot Taz 6 with firmware version v1.1.8.59 was selected as the 3D printer and Cura Lulzbot Edition 3.2.21 was the slicer. The quality, infill, travel, support, mesh fixes, special modes, and experimental settings of the Cura

Lulzbot edition slicer were left at the default "Standard Chroma Strands" settings. Specimens were printed with their cooling disabled except for Tz-1-1, which had the default print cooling of the "Standard Chroma Strands" profile. Following filament diameter measurements, 2.86 mm was used as an input in the slicer for 3D printing and all other material settings were left default unless otherwise noted. After print completion, the bed heating was stopped, and specimens were removed when the bed reached the ambient temperature (19°C) to homogenize any potential impact of annealing of the specimens due to the elevated bed temperature. The Z seam alignment, where individual extrudates start and stop, was set to random, as opposed to the default option, to stagger defects. All specimens had extra skin wall count off except for Tz 5-1. A feed rate or printing speed of 10 mm/s was used for specimens manufacturing and they had a brim of 8 mm. The manufacturing process and design parameters for specimens 3D printing are summarized in Table 2.

Table 2. Manufacturing and design parameters for 3D printing

Manufacturing/design Parameter	Value	Manufacturing/design Parameter	Value
Build orientation	ZXY	Material	ABS
Filament diameter	2.86 mm	Nozzle diameter	0.5 mm
Layer height	0.22 mm	Z seam alignment	Random
Build platform temperature	110 °C	Fill gaps between walls	everywhere
Printing speed	10mm/s everywhere	Cooling	Print cooling disabled[1]
Brim	8 mm	Part removal temp.	19 °C

[1] For Tz-1-1, fan cooling was enabled.

Per ASTM D638, the width and thickness of each specimen are measured to the nearest 0.025 mm (0.001 in). Three points are considered if the measurements are apart by less than 0.127 mm (0.005 in), while it was five for specimens with greater variability.

2.3. Thermography during 3D printing

The nozzle temperature is a critical process parameter investigated in this study and its impact on the temperature history of the deposited layers during 3D printing is of interest. A FLIR T450sc

thermal imaging camera with a resolution of 320 × 240 pixels, a thermal contrast of 30 mK, and a 30 Hz maximum frame rate is utilized to record the thermal history in 10-second intervals during 3D printing. This camera can record object temperature with a range of -20 °C to +650 °C and its accuracy is around ±2 °C for the 3D printing temperature range of this study, 19 to 260 °C. An enclosure out of black polystyrene, which has a low reflectivity, was fabricated for the LulzBot Taz 6 printer to eliminate interference from reflected hotspots and to decelerate cooling of deposited layers. Figure 3a shows the 3D printer inside the enclosure with an opening on the front door for thermal imaging. The IR camera is at 35 cm from the specimen and is placed at the same height as the specimen midpoint (angle of view, D = 0). Therefore, there is a 13.3° difference in the angle of view between the midpoint and very bottom or top parts of the specimen. Based on a study by Morgan et al. [15], this will result in less than 0.5 °C error in temperature readings for ABS material. Figure 3b displays inside the enclosure, where a tensile specimen can be seen 3D printed in the upright build direction.

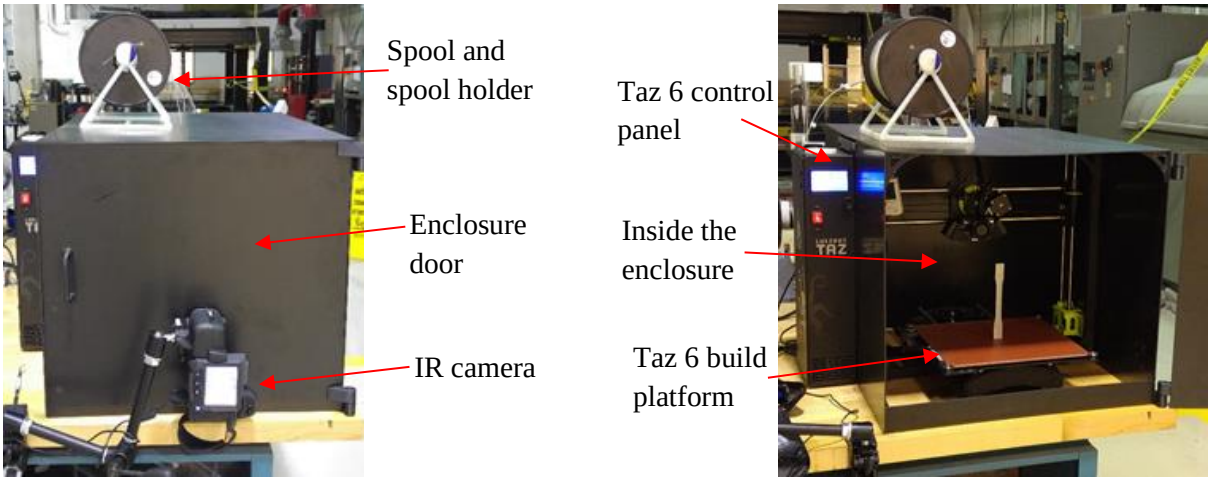

(a) **(b)**

Figure 3. The LulzBot Taz 6 printer inside a black polystyrene enclosure: (a) the outside view with the IR camera; and (b) the inside view.

Emissivity of specimens needs to be measured to analyze thermal images obtained during 3D printing, and is material and temperature dependent. For this purpose, a 3D printed ABS test piece was prepared, half of its surface was covered with black electrical tape, and was placed on the printer build platform (Figure 4a). Assuming emissivity of 0.95 for the electrical tape and knowing that both surfaces are at the same temperature, thermal imaging with the focal plane parallel with the surface of the test piece was performed to find the emissivity for ABS (Figure 4b). The emissivity of ABS at room temperature (~23 °C) was measured at 0.916, which is very close to the 0.92 value reported in the literature [15]. Emissivity at ABS glass transition temperature (T_g = 110 °C) was found to be 0.975 for smooth ABS surface and 0.987 for the rough unsmoothed one.

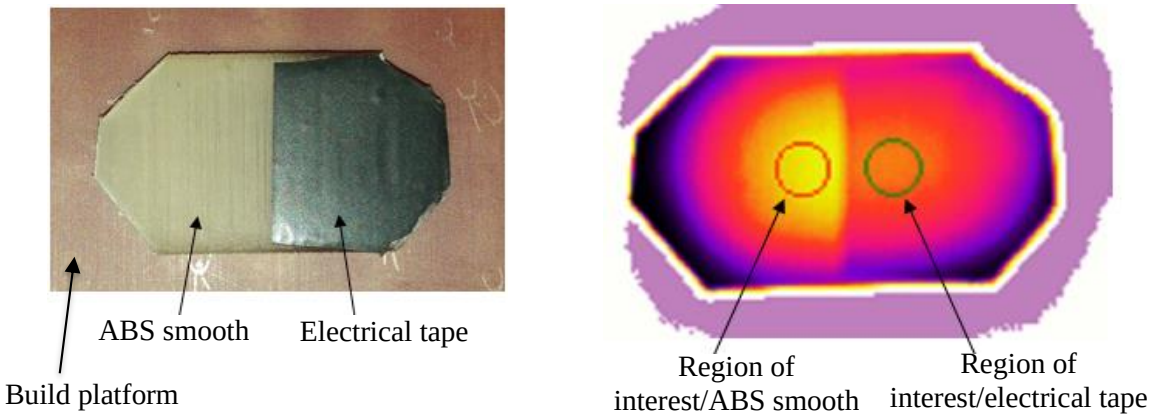

Figure 4. Technique used for measuring ABS emissivity at 110 °C: (a) 3D printed ABS piece on the build platform; and (b) thermal image results.

ResearchIR software version 4.40 was used for thermal analysis and emissivity for rough ABS surface at 110 °C was given as input. Considering the printing time, there are between 443 and 587 thermal images taken for each specimen during manufacturing. They were imported into ResearchIR software and the following procedure was performed: The thermal image enhancement was set to 90 - 250 °C; a line region of interest (ROI) was drawn along the specimen

length and through its center; and an automation script was written to extract the position, temperature, and time information along the line ROI. The noise in temperature measurements caused by the nozzle is random since the nozzle position in any given time during 3D printing is different among the specimens that have different total fabrication time. This noise was scrubbed from the data set and the time spent above the T_g was extracted for all the points along the line ROI.

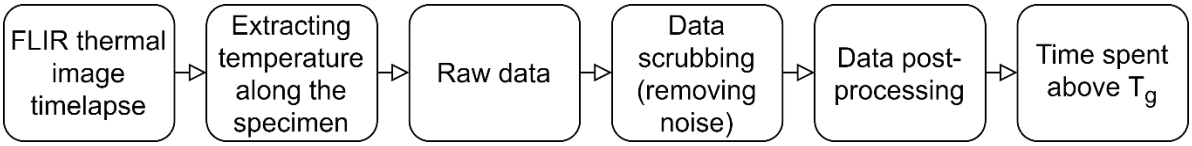

Figure 5. Automatic process for analyzing IR thermal results along the line ROI of the specimens.

The humidity and temperature inside the enclosure and outside (i.e. the laboratory environment) were measured with two Onset Hobo MX1101 data loggers. The laboratory environment is temperature controlled, while humidity changes can be significant. For the period of 3D printing specimens for this study, temperature and humidity changes were between 18 to 21 ℃ and 31.1 % to 76.3 % relative humidity (RH), respectively. Temperature and humidity were recorded up to 23 days before the start of a specimen 3D printing in five-minute intervals. Average humidity over five days was considered as the humidity during 3D printing of the specimen.

3. Results and discussion:

A United mechanical testing machine with a 500 lbf (2.22 kN) load-cell and an extensometer with 25 % strain limit was used for tensile testing. The testing speed of 5 mm/min was selected and the load-extension curve for the specimens was recorded until rupture.

3.1. The impact of the cross-sectional pattern

The first set of experiments includes specimens Tz-1-1 to 6-1, and Figure 6 shows specimens after 3D printing, indicating their weights and bottom sides.

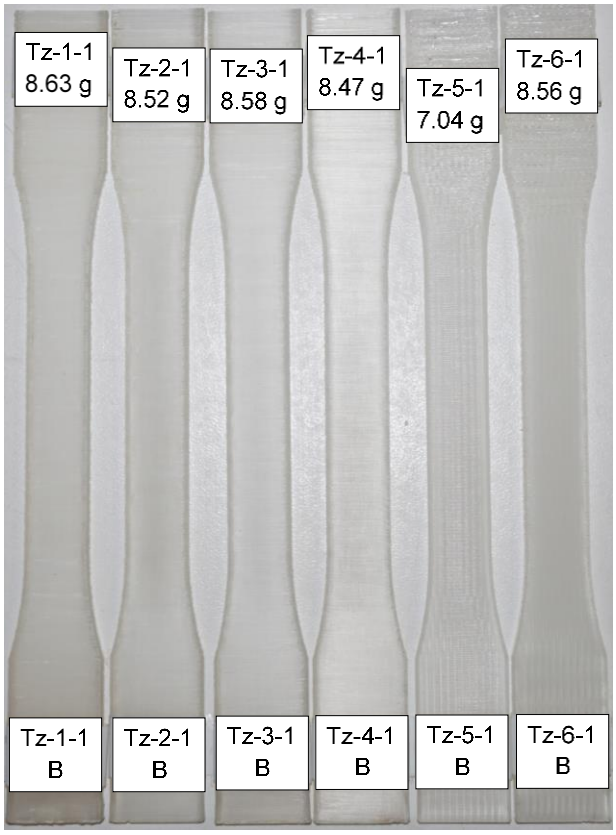

Figure 6. 3D printed specimens for the first set of experiments.

Figure 7 represents the stress-strain curve for the six specimens until failure and Table 3 summarized their Young's modulus, ultimate strength, and failure strain. Tz-1-1, 2-1, and 6-1 specimens showed a brittle failure with a maximum strain of 1.79 %, while the other samples exhibited a ductile failure.

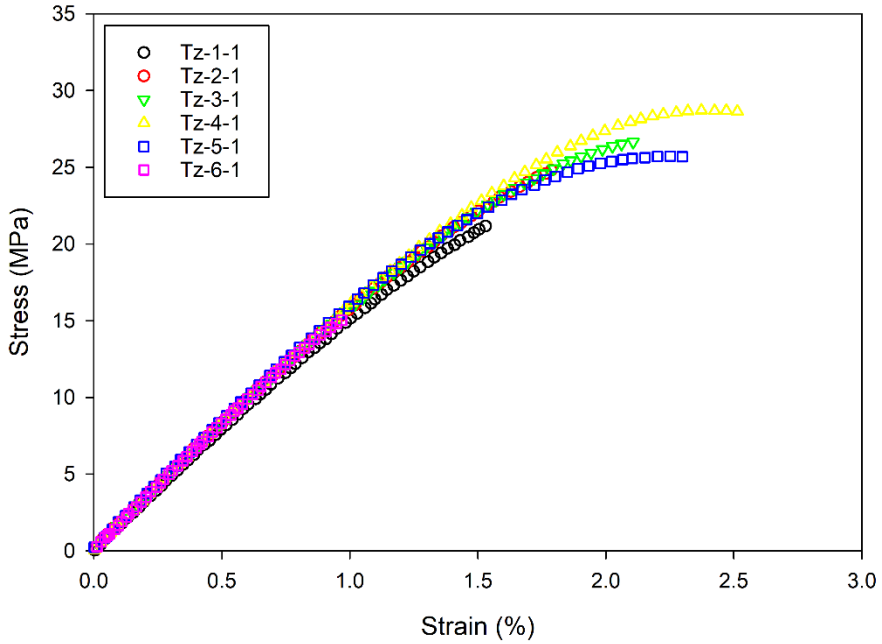

Figure 7. Stress-strain graph for the first set of experiment.

As seen in Table 3, Tz-6-1 has the highest Young's modulus among the six specimens, while Tz-4-1 exhibits the maximum ultimate tensile strength. As a result, the choice for the specimen with maximum mechanical performance and consequently optimum cross-sectional pattern is not clear. Here, the Weighted-Properties Method (WPM) developed by Farag [16, 17] is used to rank the specimens based on their performance indices calculated from simple mathematics. Specimens with the higher performance index (γ) are considered more promising for the case study. The formula for γ is provided in Eq. 1, where Young's modulus and ultimate tensile strength are normalized with the maximum value of these properties among all the specimens. In addition, it is assumed that the two properties have equal importance in this study, i.e., an equal weighting factor of 0.5.

$$\gamma = \frac{E}{\max(E)} \times 0.5 + \frac{\sigma_U}{\max(\sigma_U)} \times 0.5 \quad (1)$$

, where E is the Young's modulus and σ_U is the ultimate tensile strength for each specimen. Table 3 summarizes tensile properties of all specimens and their performance indices (γ). Per Table 3, Tz-4-1 has the highest performance index and is closely followed by Tz-3-1.

Table 3. Tensile properties for the first set of experiments.

Specimen	Young's modulus (GPa)	Ultimate strength (MPa)	Failure strain (%)	Performance index (γ) [16]
1-1	1.48	21.2	1.53	0.838
2-1	1.52	24.8	1.79	0.913
3-1	1.54	26.7	2.11	0.952
4-1	1.53	28.7	2.51	0.984
5-1	1.55	25.7	2.3	0.938
6-1	1.58	15.1	0.97	0.763
Max	1.58	28.7		
Min	1.48	15.1		

Since Tz-3-1 and 4-1 were the most promising sets of specimens, four more specimens for each were 3D printed and tested successfully. The maximum normed residual (MNR) method was used to screen Young's modulus, ultimate strength, and failure strain results for outliers. It was found that the MNR values for all test results except ultimate strength of Tz-4-1 is below or equal to the critical value, 1.715 for the sample size of five [18]. Therefore, in Table 4, all Tz-3 and -4 specimen results except ultimate strength of Tz-4-1 were used to calculate statistical values (average and Coefficient of Variation (CV)) of tensile properties. CV is the ratio of the standard deviation to the mean and is presented as a percentage. It is used in materials characterization testing to show the extent of variability in properties in relation to the mean of a sample [18].

Table 4. Tensile properties for Tz-3 and -4 specimens.

Specimen set	Young's modulus		Ultimate strength		Failure strain (%)	
	Mean (GPa)	CV (%)	Mean (MPa)	CV (%)	Mean (%)	CV (%)
Tz-3	1.53	3.63	23.6	15.4	1.81	15.9

Tz-4	1.52	1.43	24.5	0.906	2.16	11.0

A Student's t-test is performed to compare Young's modulus and ultimate strength of Tz-3 and Tz-4 specimens. It was found that there is not a statistically significant difference between Young's modulus ($P = 0.717$) and ultimate strength ($P = 0.666$) of specimens with in-to-out (Tz-3) and that of out-to-in printing (Tz-4). Visual inspection and a qualitative assessment of Tz-3 and -4 specimens showed higher surface quality for the former. This is evident from Figure 6, especially for the top sides of Tz-3-1 and 4-1 specimens. As mentioned in Section 2.2, at least three measurements of the width and the thickness were made for each specimen to the nearest 0.025 mm (0.001 in). Tz-3 specimens had an average CV of 0.17 % and 0.70 % for the width and thickness measurements, respectively, while Tz-4 specimens showed average CV values of 0.22 % and 0.84 %, respectively. A lower CV for the width and thickness measurements for Tz-3 specimens indicates lower variability in the measurement in relation to the mean, which signifies higher dimensional accuracy. Since Tz-3 specimens had better surface finish and higher dimensional accuracy compared to Tz-4 specimens, wall thickness of 1.5 mm and in-to-out printing pattern (Cross-sectional pattern a, Figure 2) were select for the rest of the study.

3.2. The impact of the nozzle temperature (no gradient)

The second set of experiments includes specimens Tz-7, -8, -3, -9 and -10 to investigate the impact of fixed nozzle temperature on the tensile properties of 3D printed specimens (Figure 8). To isolate the impact of the nozzle temperature, 13 specimens out of the total 25 that have close relative humidity levels (min: 72.4 %, max: 76.3 %, and CV: 1.7 %) were included.

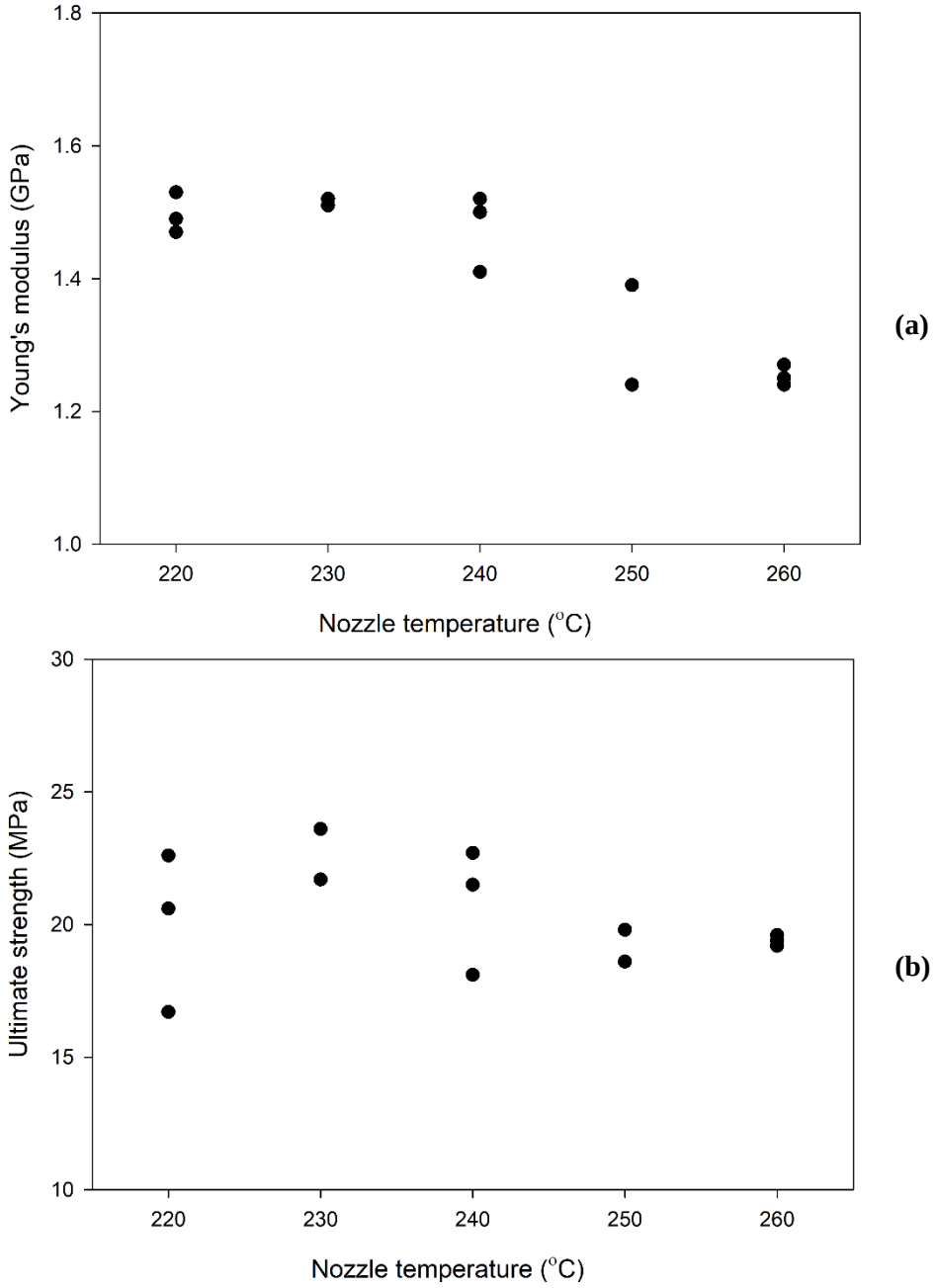

Figure 8. The impact of fixed nozzle temperature on tensile properties of 3D printed specimens: (a) Young's modulus; and (b) ultimate strength.

Per Figure 8, there is an increase in Young's modulus and ultimate strength with an increase in the nozzle temperature till 230 °C, which is then followed by a decrease in both properties. As expected, the change in ultimate strength is more significant compared to the Young's modulus. This trend has been observed by other researchers who optimized nozzle temperature for maximum

structural performance of final parts [1, 19]. Based on best curve fitting for Figure 8b, the optimum fixed nozzle temperature of 231 °C is used for the third set of experiments.

Figure 9 shows one specimen per set after 3D printing in the order of an increase in nozzle temperature from left to right, i.e., Tz-7, -8, -3, -9 and -10 with fixed nozzle temperature of 220, 230, 240, 250, and 260 °C, respectively. 3D printed specimens are more transparent for lower nozzle temperatures and the opacity increases in higher temperature values. 3D printed specimens at 220 and 230 °C were found to have the same transparency and only when the strength of specimens began to decrease at 240 °C, the specimens start to become more opaque. A relation between specimen transparency and its tensile properties needs to be investigated further that might help finding optimum 3D printing process parameters without the need to conduct extensive experimental testing.

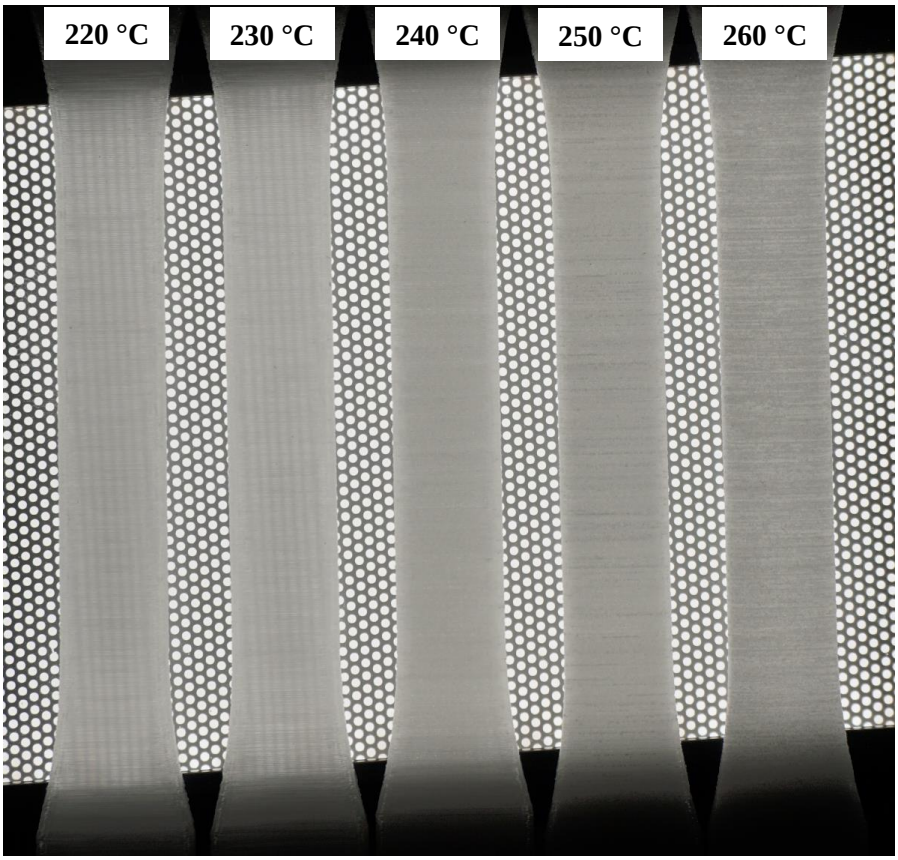

Figure 9. One specimen per set after 3D printing for different fixed nozzle temperatures.

3.3. The impact of the nozzle temperature (with gradient)

The last set of experiments includes specimens Tz-11 to -15 to investigate the impact of the variable nozzle temperature on the tensile properties of 3D printed specimens and to compare them with the baseline, Tz-8 specimens. The humidity levels for all specimens were in a close range that ensures minimum impact from humidity changes on tensile properties among specimens (min: 31.1 %, max: 40.3 %, and CV: 8.5 %). In addition, to minimize the impact of filament diameter variation through a spool, these specimens were 3D printed in sequence where one specimen was 3D printed for each set and this was repeated till all specimens were completed. Figure 10 show tensile strength and modulus of all specimens versus nozzle temperature variation. It should be recalled that the nozzle temperature is set at 231 °C in the narrow section for all specimen while it is higher in the top and bottom grip and transition regions by 5, 10, 15, 20, or 30 °C.

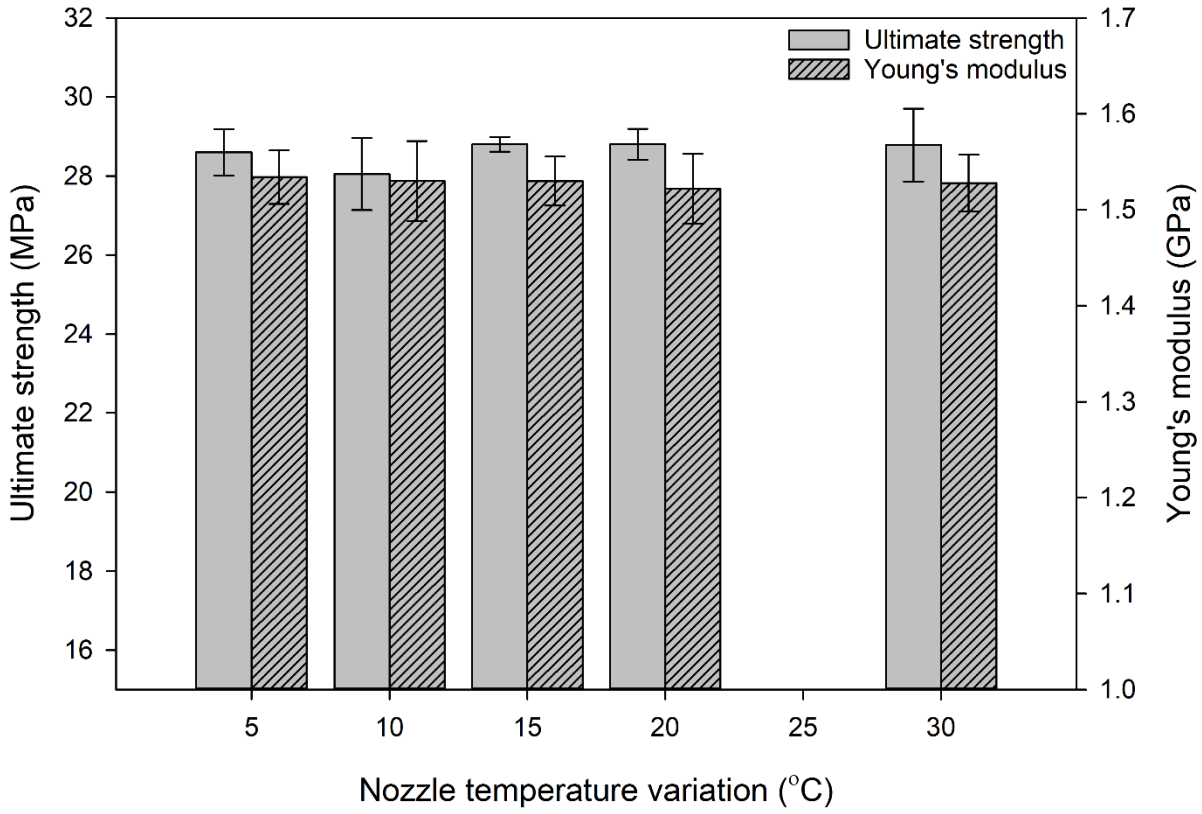

Figure 10. Tensile strength and modulus of 3D printed specimens versus nozzle temperature variation.

As it can be seen in Figure 10, there is only a slight change in tensile strength of specimens resulting from the nozzle temperature variation, while Young's modulus values are almost identical. Student's t-tests are performed to compare Young's modulus and ultimate strength of Tz-11 to -15 specimens. There are ten possible combinations for the selection of two specimen sets among the five, so a total of 10 Student's t-test for each property is performed. It was found that there is not a statically significant difference between Young's modulus (P_{min} = 0.574) and ultimate strength (P_{min} = 0.112) of specimens with different nozzle temperature variation.

Tz-8 specimens, the baseline, have an average Young's modulus of 1.50 GPa (CV: 2.9 %) and tensile strength of 23.0 MPa (CV: 5.5 %). Their average strength is noticeably lower (around 19.5 %) than the specimens with variable nozzle temperature. To understand the reasons behind this, tensile strength of all specimens versus mass and humidity were plotted in Figure 11a and b, respectively.

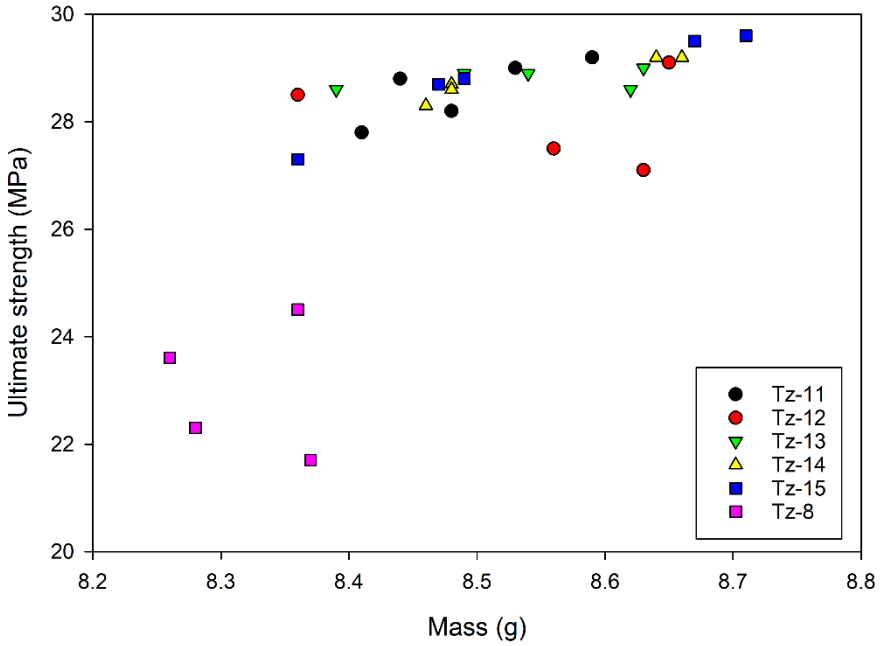

(a)

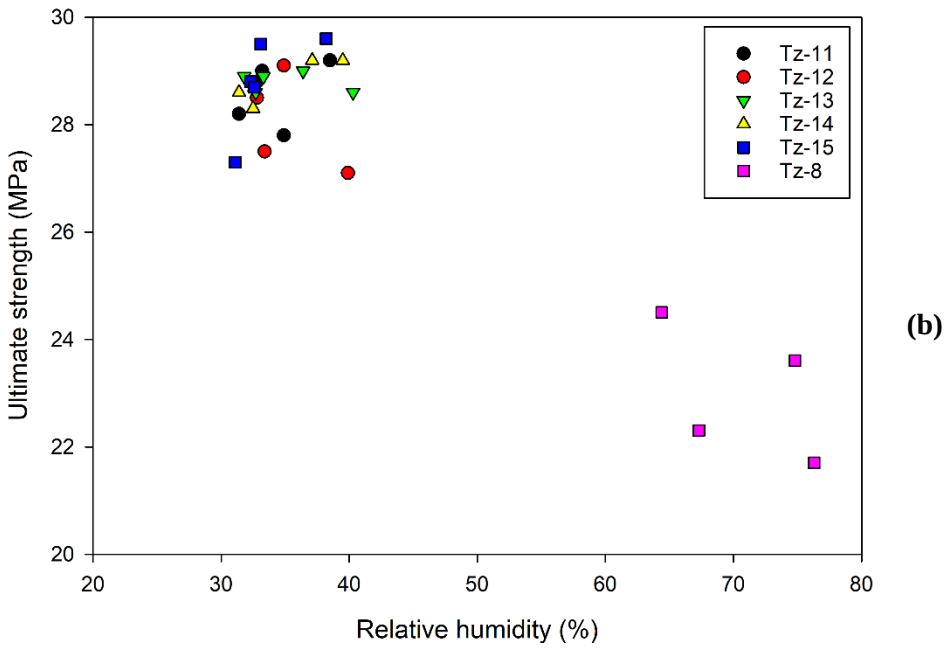

Figure 11. Tensile strength of 3D printed specimen with variable nozzle temperature and the baseline: (a) strength versus mass; and (b) strength versus relative humidity.

In general, Figure 11a shows that the baseline specimens had a lower mass and a lower ultimate strength compared to 3D printed specimens with variable nozzle temperature. However, mass is not the only contributing factor since there are specimens with a mass between 8.3 and 8.4 g that have drastically different values for ultimate strength. Figure 11b clearly demonstrates the relative humidity being the other factor, where the humidity during 3D printing of baseline specimens was much higher than the specimens with variable nozzle temperature. This shows the importance of monitoring and controlling the environment humidity during 3D printing parts.

Table 5 summarizes Young's modulus, ultimate strength, and breakage locations (Z heights) for Tz-8 and Tz-11 to -15. It should be noted that the start and the end of the narrow section are at Z heights of 54 and 111 mm, respectively. It can be seen that while all specimen sets had cases of failure outside the narrow section, the impact on their Young's modulus (maximum CV of 2.9 %) and ultimate strength (maximum CV of 5.5 %) is minimal. This is especially pronounced for Tz-13 set in which three specimens failed within and two failed outside the narrow section. The CV

for Young's modulus and ultimate tensile strength is 1.7 % and 0.6 %, respectively. This confirms that dog-bone specimens 3D printed in the upright build direction can be used to evaluate the interlayer tensile strength since the impact of failure location on Young's modulus and ultimate tensile strength is minimal. This agrees with findings from Ferrell et al. [14], in which they investigated ASTM D638 type V specimens, 3D printed in the flat build direction, and found no effect of failure in the transition area on their tensile properties.

Table 5. Tensile properties and breakage locations for Tz-8 and Tz-11 to -15.

Specimen set	Young's modulus		Ultimate strength		Breakage location (mm)				
	Mean (GPa)	CV (%)	Mean (MPa)	CV (%)	Z_1	Z_2	Z_3	Z_4	Z_5
Tz-8	1.50	2.9	23.0	5.5	107	107	110	115	
Tz-11	1.53	1.8	28.6	2.0	111	111	112	113	116
Tz-12	1.53	2.7	28.1	3.3	49	121	122	122	
Tz-13	1.53	1.7	28.8	0.6	106	109	110	121	122
Tz-14	1.52	2.4	28.8	1.4	47	47	110	110	114
Tz-15	1.53	1.9	28.8	3.2	47	105	107	113	115

3.4. Thermal imaging results

As mentioned in Section 2.3, all thermal images taken during 3D printing of specimens were analyzed, and the position, temperature, and time information were extracted automatically. Whereas previous research work analyzed temperature history of only one point [12-13], here, the temperature history of the whole specimen is found. Furthermore, for all the points along the line ROI, the time spent above the T_g is calculated as an indication of specimen local strength at those points. The number of points along the line ROI varied slightly among different specimen sets, between 186 and 195 points.

Three specimen sets are selected to discuss the thermal imaging results: Tz-8 set (baseline) is where the nozzle temperature is fixed at 230 °C, $T_0 = T_1 = 230$ °C (see Figure 1); Tz-10 is where

the fixed nozzle temperature is maximum, $T_0 = T_1 = 260$ °C; and Tz-15 set is where the nozzle temperature gradient is maximum, $T_0 = 231$ °C and $T_1 = 261$ °C. Figure 12 shows the time spent above the T_g for the specimens on the y-axis, which was considered to be a conservative value of 90 °C. The x-axis is the Z height in mm, where 0 denotes the bottom of the specimen and 165 is the top (See Figure 1). The graph shows the data extracted for one sample in each specimen set (black circles) and a line of best fit (a polynomial, blue squares) is included for clarity. The two gray dashed lines mark the beginning and the end of the narrow section at Z heights of 54 and 111 mm, respectively. The solid black lines are the breakage locations for each specimen in the set and the red line marks the average breakage location. For Tz-8 and Tz-10, two specimens failed at the same Z height of 107 and 112 mm, respectively.

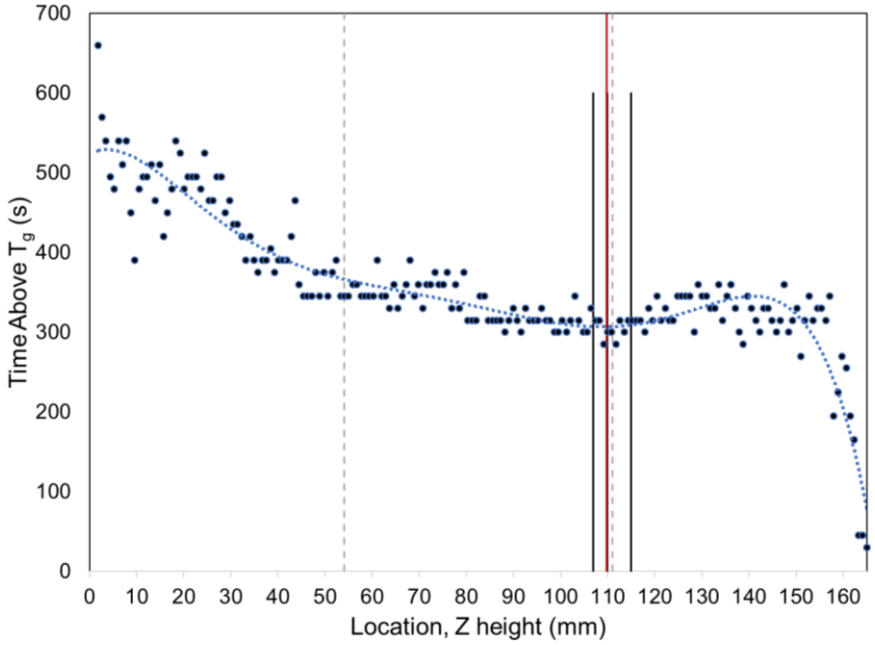

(a)

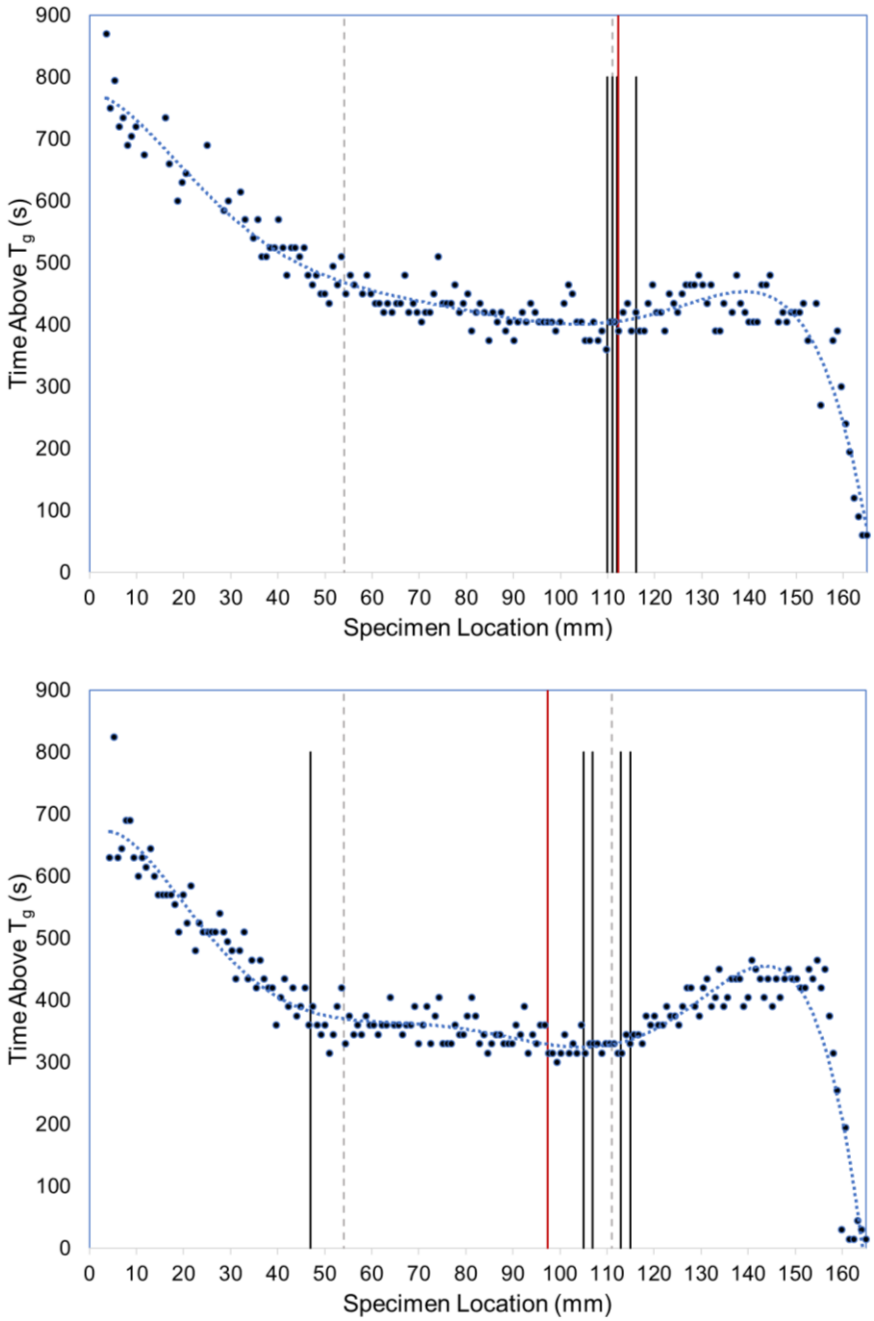

Figure 12. Time above the T_g along the line ROI of specimen sets: (a) Tz-8-1; (b) Tz-10-1; and (c) Tz-15-1.

In regions close to the bottom of the specimen, there is the maximum time spent above the T_g. There are three reasons contributing to this: (1) these regions are close to the bed, which is at 110 °C during the 3D printing; (2) there are subsequent layers that are placed on top of these regions

at the nozzle temperature of 230 or 260 °C and there is heat conduction towards the bottom of the specimen; and (3) considering the specimen's dog-bone shape, more molten material is deposited in the grip section, which means higher energy in the regions. This can be clearly seen in Figure 12a and b, where from x = 0 mm to the beginning of the narrow section, there is a continuous decrease in the time above the T_g. This is more significant for Tz-10 (Figure 12b) since it has a higher nozzle temperature of 260 °C compared to Tz-8 (Figure 12a). From the beginning to the end of the narrow section, there is a still a reduction in time above the T_g, which can be attributed to lower amount of molten material deposition in the narrow section compared to the grip areas (Figures 12a and b). From the end of the narrow section to the top of specimen, first there is an increase in the time spent above the T_g due to the increase in the cross-sectional area from the narrow to the grip and consequently an increase in the deposited molten material. After some point, there is a decrease in the time spent above the T_g and it is minimum at the very top of the specimen. After the printing completion, the nozzle moves away from the specimen and the bed heating is stopped. Therefore, it is expected that the very top of the specimen remains the shortest amount of time above the T_g (Figures 12a and b). For Tz-8 specimen set, the maximum amount of time above the T_g is 660 s, while it is 870 s for the Tz-10. It should be noted that in both cases the total print time was 128 min or 7680 s. Considering the breakage locations for Tz-8 and -10, it can be observed that they are located where the trend line reaches a minimum value, which is close to the transition area at the top section of the specimen. As a result, it seems that for FFF 3D printing of dog-bone specimens in ZXY build direction, with constant nozzle temperature and minimum testing variation, the breakage location will be in the top transition area.

The variable nozzle temperature was explored to move the minimum time above the T_g to a point in the narrow section and improve the interlayer tensile strength. Tz-15 (Figure 12c) has the highest

nozzle temperature gradient and that is why it was selected for comparison with Tz-8, the baseline, and Tz-10. For Tz-15, from x = 0 mm to the beginning of the narrow section, there is a decrease in time above the T_g. From the end of the narrow section to the very top of the specimen, there is an increase in time above the Tg followed by a decrease with the very top of the specimen being above the Tg for the minimum amount of time. These trends were observed for Tz-8 and -10 (Figures 12a and b) as well. The difference between Tz-15 and the other two specimen sets is that trend line minimum is shifted towards the center of the narrow section by about 10 mm and a larger peak is observed after the narrow section. It should be noted that the nozzle temperature in the narrow section and outside is 231 and 261 °C, respectively. As a result, the heat from the molten material deposited at 261 °C in the top transition area is conducted to several layers beneath it, deposited at 231 °C, thereby increasing their time above the Tg. Therefore, the minimum location for the trend line is not at the end of the narrow section anymore. This is shown in the breakage locations (black lines) and their average location (the red line), which are shifted towards the middle of the narrow section. For Tz-15, the maximum amount of time above the T_g is 825 s, which is expectedly higher than 660 s for the Tz-8 and is smaller than 870 s for the Tz-10 specimens set.

4. Conclusions

Interlayer tensile strength of ASTM D638 type I specimens from ABS was investigated by 3D printing them in the upright build direction. The impact of the cross-sectional pattern, and the nozzle temperature and its gradient on tensile properties of the specimen were explored. The mass, humidity, and temperature history during specimens 3D printing were recorded.

- A cross section with all walls results in maximum tensile properties, while the impact of the printing pattern (“in to out” or “out to in”) is statistically insignificant.
- For the optimum cross-sectional pattern, nozzle temperature was varied from 220 to 260 °C in 10 °C increments. There was an increase and then a decrease in tensile properties by increasing the nozzle temperature with an optimum nozzle temperature of 231 °C.
- For the narrow section, the nozzle temperature of 231 °C was kept during 3D printing the specimens, while higher temperatures were used for regions outside, i.e., the grip and transition areas. For the highest gradient, i.e., a nozzle temperature of 261 °C for the areas outside the narrow section, the breakage location was shifted towards the center of the specimens.
- The time spent above the T_g for the specimens were plotted and there was a clear relationship between its minimum and the breakage location.
- It was found that the specimen mass had a direct relation with tensile properties, while humidity had a negative impact.

In this study, time spent above the T_g was found for all specimens and it can be further analyzed to relate it to the Young’s modulus and ultimate tensile strength of the specimens using regression models. The model can be used in future optimization of 3D printing process parameters for improved interlayer tensile strength and will reduce the number of required destructive tensile testing significantly.

Funding

This work was supported by the Natural Sciences and Engineering Research Council of Canada (NSERC) under Grant RGPIN-2018-04144.

Conflicts of interest/Competing interests

The authors declare that there are no conflicts of interest.

Availability of data and material

The raw/processed data required to reproduce these findings cannot be shared at this time as the data also forms part of an ongoing study.

References

[1] Rahim, T.N.A.T., Abdullah, A.M. and Md Akil, H., 2019. Recent developments in fused deposition modeling-based 3D printing of polymers and their composites. Polymer Reviews, 59(4), pp.589-624.

[2] Fayazbakhsh, K., Movahedi, M. and Kalman, J., 2019. The impact of defects on tensile properties of 3D printed parts manufactured by fused filament fabrication. Materials Today Communications, 18, pp.140-148.

[3] Rane, R., Kulkarni, A., Prajapati, H., Taylor, R., Jain, A. and Chen, V., 2020. Post-Process Effects of Isothermal Annealing and Initially Applied Static Uniaxial Loading on the Ultimate Tensile Strength of Fused Filament Fabrication Parts. Materials, 13(2), p.352.

[4] Lin, W., Shen, H., Xu, G., Zhang, L., Fu, J. and Deng, X., 2018. Single-layer temperature-adjusting transition method to improve the bond strength of 3D-printed PCL/PLA parts. Composites Part A: Applied Science and Manufacturing, 115, pp.22-30.

[5] Zaldivar, R.J., Mclouth, T.D., Ferrelli, G.L., Patel, D.N., Hopkins, A.R. and Witkin, D., 2018. Effect of initial filament moisture content on the microstructure and mechanical performance of ULTEM® 9085 3D printed parts. Additive Manufacturing, 24, pp.457-466.

[6] Tanikella, N.G., Wittbrodt, B. and Pearce, J.M., 2017. Tensile strength of commercial polymer materials for fused filament fabrication 3D printing. Additive Manufacturing, 15, pp.40-47.

[7] Faes, M., Ferraris, E. and Moens, D., 2016. Influence of inter-layer cooling time on the quasi-static properties of ABS components produced via fused deposition modelling. Procedia Cirp, 42, pp.748-753.

[8] Morales, N.G., Fleck, T.J. and Rhoads, J.F., 2018. The effect of interlayer cooling on the mechanical properties of components printed via fused deposition. Additive Manufacturing, 24, pp.243-248.

[9] Sierra, J., Villa, D.S., Velasquez, A.M. and Villaneda, W., 2020. Relation Between Mechanical Properties and 3D Printer Configurations Parameters Using PLA at Open-Source Prusa I3. International Journal of Integrated Engineering, 12(8), pp.97-108.

[10] Zhang, Y., Yeoh, Y.C., Zheng, G. and Moon, S.K., 2018. Characterization of mechanical properties of Ultem® 9085 using FDM. Proc. Of the 3rd Intl. Conf. on Progress in Additive Manufacturing (Pro-AM 2018).

[11] Kuznetsov, V.E., Solonin, A.N., Urzhumtsev, O.D., Schilling, R. and Tavitov, A.G., 2018. Strength of PLA components fabricated with fused deposition technology using a desktop 3D printer as a function of geometrical parameters of the process. Polymers, 10(3), p.313.

[12] Kuznetsov, V.E., Solonin, A.N., Tavitov, A., Urzhumtsev, O. and Vakulik, A., 2020. Increasing strength of FFF three-dimensional printed parts by influencing on temperature-related parameters of the process. Rapid Prototyping Journal.

[13] Kuznetsov, V.E., Tavitov, A.G., Urzhumtsev, O.D., Mikhalin, M.V. and Moiseev, A.I., 2019. Hardware Factors Influencing Strength of Parts Obtained by Fused Filament Fabrication. Polymers, 11(11), p.1870.

[14] Ferrell, W.H., Arndt, C.M. and TerMaath, S., 2020. Tensile strength dependence of FFF fiber reinforced ABS on environmental conditioning. Mechanics of Advanced Materials and Structures, pp.1-14.

[15] Morgan, R.V., Reid, R.S., Baker, A.M., Lucero, B. and Bernardin, J.D., 2017. Emissivity measurements of additively manufactured materials (No. LA-UR-7-20513). Los Alamos National Lab.(LANL), Los Alamos, NM (United States).

[16] M. Farag, Materials selection for engineering design, Prentice-Hall (1997), p. 227–234.

[17] Farag, M.M., 2008. Quantitative methods of materials substitution: application to automotive components. Materials & Design, 29(2), pp.374-380.

[18] MIL-HDBK-17F "The Composite Materials Handbook." Volume 1: Polymer Matrix Composites Guidelines for Characterization of Structural Materials, ASTM International, West Conshohocken PA, 2002.

[19] Guessasma, S., Belhabib, S. and Nouri, H., 2019. Microstructure and mechanical performance of 3D printed wood-PLA/PHA using fused deposition modelling: effect of printing temperature. Polymers, 11(11), p.1778.